Geosci. Model Dev. Discuss., 6, 3085–3135, 2013
www.geosci-model-dev-discuss.net/6/3085/2013/
doi:10.5194/gmdd-6-3085-2013

Geoscientific Model Development Discussions
Open Access

Dynamic coupling of regional atmosphere to biosphere in the new generation regional climate system model REMO-iMOVE

C. Wilhelm[1,2], **D. Rechid**[1,2], **and D. Jacob**[1,2]

[1]Max Planck Institute for Meteorology, Bundesstrasse 56, 20146 Hamburg, Germany
[2]Climate Service Center (CSC), Chilehaus, Fischertwiete 1, 20095 Hamburg, Germany

Received: 17 March 2013 – Accepted: 30 April 2013 – Published: 31 May 2013

Correspondence to: C. Wilhelm (christof.wilhelm@zmaw.de)

Published by Copernicus Publications on behalf of the European Geosciences Union.

Abstract

The main objective of this study is the coupling of the regional climate model REMO to a 3rd generation land surface scheme and the evaluation of the new model version of REMO, called REMO with interactive MOsaic-based VEgetation: REMO-iMOVE. Attention is paid to the documentation of the technical aspects of the new model constituents and the coupling mechanism. We compare simulation results of REMO-iMOVE and of the reference version REMO2009, to investigate the sensitivity of the regional model to the new land surface scheme. An 11 yr climate model run (1995–2005), forced with ECMWF ERA-Interim lateral boundary conditions, over Europe in 0.44° resolution of both model versions was carried out, to represent present day European climate. The result of these experiments are compared to multiple temperature, precipitation, heat flux and leaf area index observation data, to determine the differences in the model versions. The new model version has further the ability to model net primary productivity for the given plant functional types. This new feature is thoroughly evaluated by literature values of net primary productivity of different plant species in European climatic regions. The new model version REMO-iMOVE is able to model the European climate in the same quality as the parent model version REMO2009 does. The differences in the results of the two model versions stem from the differences in the dynamics of vegetation cover and density and can be distinct in some regions, due to the influences of these parameters to the surface heat and moisture fluxes. The modeled inter-annual variability in the phenology as well as the net primary productivity lays in the range of observations and literature values for most European regions. This study also reveals the need for a more sophisticated soil moisture representation in the newly developed model version REMO-iMOVE to be able to treat the differences in plant functional types. This gets especially important if the model will be used in dynamic vegetation studies.

GMDD
6, 3085–3135, 2013

1 Introduction

Regional climate change information are nowadays derived by downscaling simulations of General Circulation Models (GCMs) with Regional Climate Models (RCMs). Long climate simulations with GCMs are limited in their horizontal resolution to values in the order of 200 km. This coarse resolution is not able to sufficiently represent local scale phenomena like extreme events, circulation characteristics due to orographic effects, structured coast lines or interlaced land use. RCMs have been developed to overcome the mentioned effects of scale and to gain more insight in the regional aspects of climate change (Giorgi, 2006). In the past years RCMs are on their road from pure atmosphere models to climate system models, by coupling to regional ocean or vegetation models. This enables the RCMs to represent biogeophysical, – chemical or – geographical aspects, like carbon cycle or land use practices in more detail.

A key advancement to achieve this task is the refined representation of surface heterogeneity in geographical terms but also in a process based manner. On the one hand this will lead to detailed process description of different surface types and the ability to model short term surface-atmosphere feedback. On the other hand long term phenomena like the carbon cycle or climatic induced land use change can be studied due to the introduction of new processes and variables.

A number of studies reveal that the land surface representation in climate models plays a vital role in the quality of the modeled climate. A change in the so called land surface scheme, which parameterizes the physical processes at the earths' surface, will mainly lead to differences in the exchange between surface and atmosphere due to modifications in heat, moisture and momentum fluxes. Avissar and Pielke (1991) show in their early study, that mesoscale atmospheric circulation could be influenced by the representation of stomatal conductance, because of the important control on the Bowen ratio. Lu et al. (2001); Steiner et al. (2009) or Davin et al. (2011) clearly showed that modifications in model land surface schemes alter the modeled climate.

GMDD
6, 3085–3135, 2013

The aim of this study is the coupling of the regional climate model REMO to a so called 3rd generation land surface scheme. 3rd generation land use schemes include a process-based representation of evapotranspiration due to the fact that they resolve plant photosynthesis and its control on stomatal conductance explicitly (Sellers et al., 1997; Pitman, 2003). The land surface scheme used is the dynamic vegetation model of the global climate model MPI-ESM (Atmosphere: ECHAM6 Stevens et al., 2013, Ocean: MPI-OM Marsland et al., 2003, Land: JSBACH Reick et al., 2013; Brovkin et al., 2012; Roeckner et al., 2003). The coupling of REMO and JSBACH introduces an interactive land surface representation into the regional climate model which brings in more complex parametrizations of vegetative processes. The new model version is called REMO-iMOVE: REMO with **i**nteractive **MO**saic-based **VE**getation.

One issue raised is how the modeled vegetation processes in JSBACH are able to react to the conditions in atmosphere and soil simulated by REMO, giving rise to comprehensible vegetation representation. Another issues discussed is in which form the new characteristics of vegetation feed back to the modeled surface climate and if the modeled values of net primary productivity of plants could be connected to measured rates.

In this study we first describe the coupled model REMO-iMOVE and then with the use of two experiments and observational datasets we evaluate the capabilities of the new model version of REMO.

2 Methods

2.1 Model description

2.1.1 REMO

The regional climate model REMO was developed at the Max-Planck-Institute for Meteorology in Hamburg (Jacob and Podzun, 1997; Jacob, 2001) from parts of the DWD

GMDD
6, 3085–3135, 2013

EM-DM model (Majewski, 1991) and ECHAM4 (Roeckner et al., 2000). It is under constant development to keep the model up to date with the latest advancements in climate science. The model constituents are described in various literature (e.g. Pfeiffer, 2006; Kotlarski, 2007; Teichmann, 2010).

As this work is discussing the influence of extending REMO by implementing a so-called 3rd generation surface scheme, we describe the currently used surface scheme of REMO in the following.

REMO in the version used here (REMO2009) incorporates a 1st generation land surface scheme. Physical surface characteristics regarding soil and vegetation (soil texture, leaf area index and vegetation ratio) are derived from FAO data (Zobler, 1986), a dataset called LSPII (Hagemann et al., 1999; Hagemann, 2002) and a dataset of major ecosystem types (Olson, 1994). The derivation of snow-free surface albedo from MODIS satellite data is described in Rechid et al. (2009). The geographic distribution of vegetation and it's phenology is prescribed and static throughout the whole simulation.

The hydrological properties of the soil are derived from a relatively coarse source and comprise a simple bucket soil water scheme (Kotlarski, 2007). Soil temperatures are calculated from diffusion equations solved in five discrete layers with zero heat flux at the bottom (10 m depth) according to the scheme of Warrilow et al. (2007).

2.1.2 REMO-iMOVE

GCMs have been coupled to 3rd generation surface scheme to be able to dynamically simulate interactions of vegetation and climate. At the Max-Planck-Institute for Meteorology the 3rd generation surface scheme JSBACH was developed for the GCM ECHAM6, to enhance the capabilities of the GCM towards an ESM. JSBACH has an advantage over models of the LPJ-family (Sitch et al., 2003) and other state of the art surface schemes, because it is able to exchange surface fluxes on a model time step basis (approx. 10 min for GCMs, approx. 2 min for RCMs). This enables JSBACH to accurately model the daily cycle of surface atmosphere interaction. This was the main reason to use JSBACH to couple it to REMO. A further advantage of JSBACH is the

GMDD
6, 3085–3135, 2013

coding similarity to REMO. REMO was descended from an older ECHAM version, so the technical coding aspects between REMO and JSBACH have been beneficial for the development.

The coupled version REMO-iMOVE received the most important biophysical parametrizations for vegetation modeling of JSBACH. In the following we explain the parts built into REMO, as well as the coupling methodology.

One of the most distinct advancement of REMO-iMOVE is the introduction of the concept of plant functional types (PFTs). This concept implicates a mosaic representation of surface vegetation on biome scale, which allows to divide the vegetation types of a single grid cell into 16 different PFTs. The 16 PFT classes are differentiated by their major biogeophysical peculiarities into tropical broadleaf evergreen (PFT 1) and deciduous trees (PFT 2), temperate broadleaf evergreen (PFT 3) and deciduous trees (PFT 4), evergreen (PFT 5) and deciduous coniferous trees (PFT 6), coniferous (PFT 7) and deciduous shrubs (PFT 8), C3 (PFT 9) and C4 (PFT 10) grasses, tundra (PFT 11), swamp (PFT 12), C3 (PFT 13) and C4 crops (PFT 14), urban (PFT 15) and bare land (PFT 16).

The distribution of vegetation cover into the PFT classes is based on the GLOBCOVER 2000 dataset (GLC2000), which is available in 1×1 km horizontal resolution (Bartholome and Belward, 2005). The classification of GLC2000 contains not only classes which can closely be mapped into PFTs (e.g. needleleaf trees), but also contains mixed vegetation classes (e.g. mixtures of trees and shrubs), which need a further separation into PFTs.

On the basis of the fact that vegetation cover is closely connected to climatic regimes (Schultz, 2002), we can connect the vegetation cover information of GLC2000 to the ecosystem classification of Holdridge (Holdridge, 1964). With these two information sources an allocation of the mixed GLC2000 classes into PFTs is possible.

The ecosystem classification of Holdridge uses the parameter biotemperature, which is computed according to Eq. (1). Another parameter used is the annual precipitation

GMDD
6, 3085–3135, 2013

sum.

$$\text{Biotemperature} = \left[\sum_{i=1}^{12} \text{monthly\_mean\_temp}(i)\right] /12 \quad (1)$$

Biotemperature and precipitation sum were computed using the climatological mean of CRU3 gridded observation data from 1970 to 2000 (Mitchell and Jones, 2005). The resulting ecosystem type classification based on Holdridge is shown in Table 1.

For each of the classes of the GLC2000 dataset we can derive a matrix, based on the ecosystem classes in Table 1 to allocate the mixed vegetation types into PFTs according to the prevailing climate conditions at the grid box location. Table 2 gives an example on how a GLC2000 class "mosaic vegetation" (grassland/shrubland/forest (50–70 %)/cropland (20–50 %)) is allocated to PFTs. In a wet forest climate type for example (precipitation sum of 1000–2000 mm/biotemperature of 6–12 °C), the surface cover of the GLC2000 class would be splitted into 40 % of PFT 13 (C3 cropland), 25 % of PFT 4 (deciduous trees), 25 % of PFT 5 (evergreen coniferous) and 10 % PFT 3 bzw. 4 (C3/C4 grass).

All the allocation tables, to translate GLC2000 classes into PFTs, can be received upon request, but are not considered essential for the understanding at this point.

Surface radiation fluxes are determined by the surface albedo. Therefore the albedo representation of the surface plays a vital role in climate models. In REMO-iMOVE the whole grid cell albedo for the land part is composed of the albedo of vegetation, bare soil and snow and is computed at each model time step. Vegetation albedo is fixed for each PFT. Bare soil albedo is determined by combining the distribution of soil types (Harmonized World Soil Database (FAO/IIASA/ISRIC/ISSCAC/JRC, 2009) with satellite derived albedo information for soil types in their dry state (Tsvetsinskaya et al., 2011). Albedo characteristics of soils, which are not present in the study of Tsvetsinskaya et al. were taken from Bonan (2002). To get a more realistic soil albedo, the raw soil albedo values (α_{soil}) are mixed with a value for litter albedo (α_{litter} = constant = 0.12), by using a function depending on the PFTs which are found

GMDD
6, 3085–3135, 2013

in the grid cell. For the details compare Eq. (2). The litter factor is only applied, if the net primary productivity of the previous year is positive, otherwise it is assumed that no litter is present on the tile. This assumption is crucial for desert environments were vegetation develops only if moisture is present.

$$\alpha_{\text{soil+litter}} = \frac{\alpha_{\text{soil}} + \chi \times \alpha_{\text{litter}}}{\chi + 1} \tag{2}$$

with χ dependent on PFT (see Table 6).

Soil moisture also plays a role in changing the albedo of soils. Peterson et al. (1979) show a linear correlation between albedo decrease due to soil wetting. They also state: "the lighter the soil, the greater the loss in reflectance". Muller and Decamps (2001) also found a slight linear relationship of the albedo decrease due to wetting as well as a spread in the reflectance behavior due to different soil textures. In REMO-iMOVE we use a negative exponential relationship between increasing soil moisture and albedo decrease. The ratio between the actual soil moisture WS_{act} and the soil moisture of the soil at field capacity WS_{fcap} scales the relationship, compare Eq. (3).

$$\alpha_{\text{soil+litter-wetted}} = \alpha_{\text{soil+litter}} \times \exp^{-0.1 \frac{WS_{act}}{WS_{fcap}}} \tag{3}$$

We assume that above field capacity the soil is darkest, even when wetted further. The lower limit of the soil moisture in this context is given by the wilting point, where we assume that the soil looks dry, therefore is brightest. Here $\alpha_{\text{soil+litter}}$ is used.

The field capacity and wilting point percentage values referred to in the paragraph above, are related to the maximum water holding capacity of the soil volume of a grid box. This maximum water holding capacity is determined by the soil substrate. The amount of water that is available for plants is dependent on their root characteristics. In REMO as well as in REMO-iMOVE the parametrization described in Hagemann (2002) is used for determining the water holding capacity of a grid box from soil substrate and vegetation root characteristics.

GMDD
6, 3085–3135, 2013

From the radiation interaction with the soil and vegetation due to reflectance issues, we come to the radiation interaction within the plant canopy, plant productivity and stomatal control. All parts are taken from JSBACH.

The radiation interaction within the canopy is modeled by the two stream approximation proposed by Dickinson (1983) and Sellers (1985). In this theory it is assumed that the distribution of scatterers in the canopy is completely homogeneous, so that the radiation distribution within the canopy is horizontally invariant. The product of this routine is the fraction of photosynthetically active radiation absorbed by the plants in the grid box (fAPAR). Having fAPAR modeled, the photosynthetic rate and dark respiration is computed using the amount of soil water, temperature, atmospheric pressure, and the PFT-specific values for leaf area index (LAI), electron transport capacity and carboxylation rate, as well as the atmospheric CO_2 concentration. The computation of the photosynthetic rate follows the standard approach used in vegetation modeling, which is the model of Farquhar et al. (1980) for species characterized by the C3 photosynthetic pathway and the model of Collatz et al. (1992) for species using the C4 photosynthetic pathway. The photosynthesis rate determines the amount of plant transpiration based on the amount of stomata aperture of the vegetation. The parametrization of stomatal control follows a model called BETHY described in Knorr (1998).

The net primary productivity of the vegetation cover in a model grid cell is computed, by substracting the dark respiration from the photosynthesis rate for each PFT fraction.

The following explanation of the interactive phenological scheme of JSBACH have been acquired by personal communication of the authors and C. H. Reick, T. Raddatz and R. Schnur of the Max Plack Institute for Meteorology, Hamburg, in the years 2010 and 2011.

The interactive phenological scheme is driven by the atmospheric forcing and the soil hydrological state and follows a general logistic growth approach in the form:

$$\frac{\mathrm{d}\Lambda}{\mathrm{d}t} = k\Lambda\left(1 - \frac{\Lambda}{\Lambda_{\max}}\right) - p\Lambda \tag{4}$$

GMDD
6, 3085–3135, 2013

with

Λ : LAI

Λ_{max} : max. LAI

k : growth rate

p : shedding rate

Four different phenological characteristics are captured by this approach: summergreen, raingreen, grasses and crops. The fifth "phenology" is the evergreen type which assumes always the maximum LAI for the PFT.

The raingreen phenology depends only on the plant available water. The PFTs start to increase their LAI value (start to grow), if the plant available water exceeds the wilting point level. If the plant available water is above the wilting point level in later time steps and the day before productivity is positive, raingreen plants grow further at the logistic growth rate. If the water level drops below wilting point, raingreen PFTs die back also at the logistic rate with $p > k$.

The phenology for grasses is dependent on the plant available water, as well as on a temperature threshold. If the plant available water exceeds the wilting point and the temperature is above 5 °C, the grass PFTs start to grow. Grass PFTs grow further, at the logistic growth rate ($k > p$) if the day before NPP rate is positive, plant available water is above wilting point and the temperature threshold is exceeded. If the day before NPP rate is negative but water and temperature are fine, grasses do not grow further, but lose a bit of LAI ($p > k$). Grass PFTs die back if either water or temperature are below the mentioned threshold.

The crop phenology is modeled like the grass phenology with the supplementary, that the temperature needed for growth has to be larger than 10 °C. This prevents crops to start growing early in spring. The growth rate k for crops depends on the day before NPP rate:

$$k = q \times \mathrm{NPP}_{+} \times \mathrm{SLA} \quad (5)$$

GMDD
6, 3085–3135, 2013

with

q : 0.8

SLA : 0.45

NPP_+ : NPP for NPP > 0

Crops are harvested and the LAI is set to a minimum values of 0.1, when the heat sum threshold is met. The heat sum specifies the sum of daily mean temperature exceeding 6 °C. This sum begins counting at the first day of growth. The exceeding temperature is only summed up if the day before NPP rate was positive. This concept makes sure that in warmer climates crops will be harvested earlier, if enough water was present.

The summergreen phenology depends only on soil and air temperatures and can be subdivided into three phases:

- growth phase (spring), characterized by non-zero k and $q = 0$
- vegetative phase (summer), growth is zero and leaf shedding is small
- rest phase (autumn and winter), rapid leaf shedding, growth zero

The most important points in time to model are the date when growth starts (spring event) and the date when plant rest begins (autumn event). The begin of the vegetative phase is modeled by heat summation like in the crop phenology. The spring event is determined following the alternating model of Murray et al. (1989) and depends on the magnitude of daily mean temperatures since the autumn event. The autumn event is triggered by the soil and air temperatures. If the soil temperature falls below a threshold of 10 °C and the daily mean air temperature is below the soil temperature, the rest phase begins.

Another important point that is improved in REMO-iMOVE is the parametrization of bare soil evaporation. In REMO, bare soil evaporation is allowed only if the soil water

GMDD
6, 3085–3135, 2013

content exceeds 90 % of the maximum bucket fill (WS_{max}). REMO-iMOVE admits bare soil evaporation also if the soil water content is below the 90 % threshold, and couples the resistance against evaporation from the bare ground (η_{bare}) to the bucket fill and the area of bare soil in the grid cell. The values of η_{bare} follow a model inherent logic, the higher the values, the less water is evaporated from bare soil.

The method built in REMO-iMOVE, allows bare soil evaporation at maximum rate ($\eta_{bare} = 20\,\%$), if water is available in the soil (35 % of WS_{max}) and if the vegetation cover is minimal (LAI < 1). Here the shadowing of the soil due to plants is only fractional. If bare soil shadowing by plants is abundant (LAI ≥ 1), the resistance against bare soil evaporation will take a lower value ($\eta_{bare} = 45\,\%$) if enough water is present (> 90 % of WS_{max}). If the water availability is limited (< 90 % of WS_{max}) the resistance against bare soil evaporation will increase ($\eta_{bare} = 55\,\%$). If the soil water drops to minimum values (< 35 % of WS_{max}), the bare soil evaporation is rather inhibited ($\eta_{bare} = 90\,\%$).

The stated method brings in some improvements over the standard parametrization in REMO, even if it is far from perfect. A clear disadvantage of the scheme is, that it does not capture the transition zones in bare soil evaporation regimes. This can only be overcome by a soil hydrological parametrization with a multi layer soil model, but that was beyond the scope of this coupling study.

2.1.3 Coupling between REMO and JSBACH

REMO and JSBACH are technically very similar. This similarity made it possible to implement JSBACH as a subroutine of REMO. Therefore the coupling between the two models could be realized on a model time step basis without loss of computational performance. Figure 1 shows the concept of the coupling and the computations done by the iMOVE (JSBACH) sub-model. Here we show only the most important parameters and processes. In the left box the directly concerned processes and parameters of standard REMO are shown in blue and grey. On the right hand side the new processes and parameters are shown in green, yellow and grey. Green parameters mean that

GMDD
6, 3085–3135, 2013

a quantity is processed for each PFT of a grid cell. Yellow parameters are accumulated as a weighted PFT average for the grid cell and reported back to REMO.

The canopy absorption model of iMOVE gets the photosynthetically active radiation of REMO and together with the LAI for each PFT the fAPAR is computed. fAPAR is used together with atmospheric CO_2, pressure, temperature, atmospheric moisture and LAI to derive the water unlimited photosynthesis rate and unstressed stomatal conductance. The water stress factor is computed using the soil water content of REMO (the hydrological soil parametrization in REMO and ECHAM6 are similar). The photosynthesis rate and stomatal conductance is computed using unstressed quantities combined with the computed water stress factor. The actual photosynthesis rate is the basis for NPP. The actual stomatal conductance is given back to REMO to compute the surface evaporation fluxes. NPP and the model time are used in the phenology model to derive the updated LAI. The surface vegetation ratio (VGR) is derived from the LAI via Beers extinction law on PFT basis for the whole grid cell. The grid cell albedo is updated using soil albedo, vegetation albedo, snow cover and the water fraction, if open water is present in the grid cell. The grid cell roughness length (Z0) is computed using vegetation and soil roughness length on weighted PFT basis. The updated and accumulated physical surface parameters for each grid cell VGR, LAI, albedo and Z0 are passed to the surface flux computations of REMO.

This surface scheme and the coupling method is able to interact with the atmosphere and hence adjusts the surface parameters based on the atmospheric forcing. In turn it feeds back reactions of the surface to the surface flux computations and so influences the atmospheric state.

3 Experiments

To check the performance of REMO-iMOVE in comparison to standard REMO we conduct two 11 yr simulations under past climate conditions from 1995 to 2005 for the European continent in 0.44° resolution. The models are forced with so-called perfect

GMDD
6, 3085–3135, 2013

lateral boundary conditions ECMWF ERA-Interim (Simmons et al., 2006) in 0.7° resolution. To bring the soil thermal properties into equilibrium with the climate, a soil spin up of three years is run beforehand. The soil hydrological conditions are not put into equilibrium to check the adjustment of vegetation cover in the first year. Figure 2 depicts the orography of the model domain projected on a globe.

4 Reference datasets

As reference to compare the climatic parameters of the two model runs against, various observational datasets were used. Unfortunately not all datasets were available for the whole simulation period. For datasets not available for the whole period, the period present in the observational dataset was compared. For each observed parameter the monthly means values over all years available were compared against the simulations. All observational datasets were remapped to the model grid at 0.44° resolution.

As reference dataset for 2 m temperature we utilize the gridded datasets of the Climate Research Unit version 3.0 (CRU) at 0.5° resolution (Mitchell and Jones, 2005) and the observational dataset of the EU FP6 Ensembles project (E-OBS) at 0.5° resolution (Haylock et al., 2008), to get an observation data spread for this parameter. As observational dataset for precipitation the CRU version 3.0 product at 0.5° resolution and the Global Precipitation Climatology Centre (GPCC) data at 1.0° resolution (Rudolf and Schneider, 2004) are used, also to get a spread in the observations for this volatile parameter. Surface latent heat fluxes are compared against gridded FLUXNET data at 1 km resolution resolution, processed by Jung et al. (2011). The dataset is available for the years 1996 to 2001, which is used for the comparison. The model LAI cycle is compared against the CYCLOPES LAI product at 1 km resolution (Baret et al., 2007). Uncertainties in satellite LAI estimations are known and result mainly from unstable retrieval of LAI from surface reflectances. These can bias satellite derived LAI magnitudes under some circumstances by 50 % (Garrigues et al., 2008). Despite these uncertainties CYCLOPES data are evaluated against in-situ data and

GMDD
6, 3085–3135, 2013

show good agreement for all land cover types except dense vegetation where LAI is underestimated (Weiss et al., 2007; Garrigues et al., 2008). To evaluate the LAI we employed the described CYCLOPES data for the years 2002 and 2003.

5 Results

5.1 Comparison between REMO2009 and REMO-iMOVE

The modifications in the model REMO-iMOVE result mainly in changes of surface characteristics like albedo, LAI, vegetated part of the grid cell, roughness length, stomatal conductance or plant available soil water. The surface parameters play a vital role in modeling the surface climate as mentioned above. In this section, we will on the one hand compare the two model versions REMO2009 and REMO-iMOVE in respect of their ability to model the climate of the 10 yr period 1996 to 2005. On the other hand we will introduce the new model features of REMO-iMOVE and their importance.

At first, an overview for the changes in the 2 m temperature, precipitation and latent heat flux characteristics is given. In this more general insight we will identify areas, where the model versions differ to a large degree. In a second step, we will analyze the areas where the differences in the model versions are most distinct, to in-depth understand the reasons. In the second part we will make use of the climate classification of Koeppen–Geiger (Koeppen, 1900) to distinguish between different climatic regimes subdivided by regional characteristic units of European landscapes. Figure 3 shows the distribution of climate types and the landscape units. The climate types are briefly explained in Table 3.

5.1.1 Overview: 2 m temperature

In Fig. 4 a, b the deviation in 2 m temperature (2 m-T) in Kelvin to CRU is shown. In the winter months a pronounced large scale warm bias reaching up to 3 K over Scandinavia is visible. This bias is reduced in extent in January, but still high in magnitude.

GMDD
6, 3085–3135, 2013

It declines till April and reappears again in November. Contrasting to the warm bias, a large scale cold deviation is evident in most parts of the north eastern domain. The cold deviation with magnitudes of partly more than −3 K begins to appear in December and strengthens in magnitude and extent till April. It is more pronounced in REMO2009 than in REMO-iMOVE, where especially in March and April the magnitude and extent is significantly reduced. A large scale cold bias in May in REMO2009, also in the north eastern part of the domain reaches values up to −2 K. This deviation is largely reduced in extent and magnitude in REMO-iMOVE.

The Balkans and the north eastern shore of the Black Sea show a warm deviation with magnitudes up to 2.5 K from December to March in REMO2009. This deviation is reduced in extent and magnitude in REMO-iMOVE, where it totally disappears in March. The months April, May and June are simulated well in both version, nevertheless REMO-iMOVE shows slight more overestimation up to 1 K in western and central Europe than REMO2009. Beginning in July REMO-iMOVE shows a significant warm feature in magnitude up to 2.5 K over south western Spain, Italy, the Balkans and the north African shoreline. REMO2009 also simulates the warm feature in southern Spain, Italy and north Africa. In August the warm biases in both model versions still persist, with a significant warm bias over the Balkans unique for REMO-iMOVE. The bias in south western Spain in contrary is relieved in REMO-iMOVE compared to REMO2009. September and October show a large scale warm bias in REMO-iMOVE over central Europe reaching magnitudes up to 1.5 K. These features are less pronounced, but present, in REMO2009. In the summer month June, July and August a cold deviation is visible in REMO2009 over whole eastern Europe with magnitudes up to −1.5 K. This cold bias is no longer evident in REMO-iMOVE. A large scale cold feature over the Saharan belt is visible in both model versions all over the year with deviations reaching more than −3 K. When comparing to the E-OBS dataset (not shown) the main deviations described show the same patterns even if the magnitudes differ slightly.

GMDD
6, 3085–3135, 2013

5.1.2 Overview: precipitation

In Fig. 5a, b the deviation of precipitation in percent to CRU observational data is shown. The first feature visible is the strong deviation in the Saharan belt, which is produced when looking at relative differences of very small numbers in percent. A quantitative comparison is usually not made for such regions and will also not be made here.

In winter and early spring till April, both models show similar deviation patterns with a large scale overestimation of precipitation by 40 to 60 % for whole central and northern Europe. An exeption from this general overestimation in winter are the British Isles, which show a slight underestimation with magnitudes up to 40 to 60 % over the whole year. Also in mountainous terrain (Alps, Balkans, Caucasus) and partly in Spain and Italy an underestimation of precipitation is depicted with magnitudes ranging up to 80 %. In May, the conform picture for both models change. While REMO2009 still shows an overestimation in whole central and northern Europe, REMO-iMOVE simulates an underestimation of precipitation over the northern Balkans. This feature persists and grows in magnitude and extent until September and October. REMO2009 simulates an equally large dry bias in extent and magnitude in August, September and October also for the Balkans region. In September REMO2009 shows an intensive dry bias located over the Balkans, with large scale magnitudes up to 100 % less precipitation. This bias is apparent in REMO-iMOVE also, but it's magnitude is reduced in most parts. Italy and Greece fall under a distinct dry bias in both model versions in autumn, with deviations up to 80 % less precipitation amount.

In Fig. 6 the deviation in precipitation to GPCC observational data is shown. As general noticeable feature, the overestimation of precipitation over central and northern Europe remains, equal to the picture shown when compared to CRU, although the deviation magnitude is smaller and regional differences occur.

The period December to March in contrary, shows an underestimation in parts of western and central Europe in both models.

GMDD
6, 3085–3135, 2013

An important point is also the reduction of the dry bias over mountainous areas, especially the Alps and the Caucasus, these areas in contrary to CRU show an overestimation when compared to GPCC. The summer and autumn dry bias over the Balkans and central Europe in REMO-iMOVE persists in this comparison. A remarkable feature is the intensive dry bias in REMO2009 over the Balkans with magnitudes up to 100 % decreased precipitation. Although the bias is evident in REMO-iMOVE also, its magnitude is strongly reduced. The autumn dry bias in Italy and Greece is also a common feature for both models, when comparing to GPCC.

5.1.3 Overview: latent heat flux

Figure 7a and b show the deviation of the simulated latent heat flux against gridded FLUXNET data. Beginning in November until March, deviations are small due to the energy limitation for evaporation by incoming solar radiation. From May until August REMO2009 severely overestimates the latent heat flux over the whole European continent in magnitudes by more than $+50\,\mathrm{W\,m^{-2}}$. The extreme cases can be seen in the Mediterranean region and Kazakh-Steppe regions. In REMO2009 an underestimation takes place in late summer and autumn in the Mediterranean and north African regions. REMO-iMOVE shows similar overestimations like REMO2009, whilst magnitudes fall behind the values of REMO2009 except in Turkey and northern Spain. In July and August, both model version show an underestimation in the Hungarian Basin and the Danube delta area. This feature is more pronounced in REMO-iMOVE as it is in REMO2009. September and October show a slight large scale underestimation of latent heat flux over western and central Europe and the Balkans in REMO-iMOVE. REMO2009 shows such a behavior over Spain. A distinct difference between the model versions, is the simulated result in May over northern Scandinavia. Here REMO2009 shows a slight overestimation of up to $+20\,\mathrm{W\,m^{-2}}$, when REMO-iMOVE shows the opposite.

In Sects. 5.1.1, 5.1.2 and 5.1.3 two main regions can be identified, where differences in the model versions REMO2009 and REMO-iMOVE are most pronounced:

GMDD
6, 3085–3135, 2013

– The north eastern parts of the domain, where the cold bias in REMO2009 from February to May is reduced in magnitude and extent in REMO-iMOVE.

– The Balkans, Hungarian Lowlands and the west coast of the Black Sea, where the warm bias of REMO2009 from July until October – the so called summer drying phenomenon – is increased in extent and strength in REMO-iMOVE. This feature can be entangled with a distinct precipitation and latent heat flux reduction in REMO-iMOVE.

In the next part, we will discuss the reasons for the differences in the model behavior, before we will introduce and evaluate the new model features of REMO-iMOVE.

5.1.4 Reduction of the cold bias in the north eastern part of the domain in winter

The reduction of the cold bias in the north east of the domain in REMO-iMOVE is based on the fact that the forest cover in that part is increased by 30 to 40 % in a large areal extent (Fig. 8). If forest is present in snow covered landscapes, the albedo of snow which normally uniformly covers the surface is reduced, resulting in less effective radiation reflection. The snow albedo in the model if forest is present $\alpha_{\text{snow}_{\text{forest}}}$ is a function of the surface temperature and the forest fraction f_{forest} of the grid cell. For $T_s \leq 10\,^{\circ}\text{C}$ the albedo is fixed to a maximum value for $\alpha_{\text{snow}_{\text{forest}}}$. For $-10\,^{\circ}\text{C} < T_s < 0\,^{\circ}\text{C}$ the snow albedo increases linearly until the minimum value of $\alpha_{\text{snow}_{\text{forest}}}$ is reached at $T_s = 0\,^{\circ}\text{C}$. The maximum and minimum values of $\alpha_{\text{snow}_{\text{forest}}}$ depend further on the forest fraction f_{forest} and vary from 0.4 to 0.8 and from 0.3 to 0.4 respectively. The lower value is valid for maximum forest fraction $f_{\text{forest}} = 1$, the higher value for minimum forest cover $f_{\text{forest}} = 0$ (Kotlarski, 2007). Figure 9 shows the differences in surface albedo between the model versions and the snow depth in REMO-iMOVE (REMO2009 is not shown but is almost equal). The distinct decrease in reflectance is correlated to the presence of snow and the increase in forest fraction.

The snow reduction of the masking effect and the decrease of soil albedo if snow is present cannot be the reason for the reduction of the cold bias in May. Here, no

GMDD
6, 3085–3135, 2013
REMO-iMOVE
C. Wilhelm et al.

snow is present and the albedo is increased in REMO-iMOVE. The 2 m temperature increase in REMO-iMOVE is correlated with a decrease in LAI (not shown). This results in a change of the Bowen ratio towards the sensible heat flux and less evaporative cooling of surface temperatures.

5.1.5 Increase of the warm bias in central east Europe from July to October

Mainly the areas in the Balkans region, the Hungarian lowlands and the west coast of the Black Sea are under the influence of a distinct increase in 2 m temperatures in REMO-iMOVE from July until October. The areas showing the warm deviation, correlate with a drop in LAI and vegetation ratio (VGR) in REMO-iMOVE (Fig. 10). This decrease in vegetated area decreases the effective amount of transpiration and changes the Bowen ratio towards the sensible heat flux, causing a temperature increase. The change in the Bowen ratio causes a drying of the lower atmosphere. The lower atmospheric moisture provides an important part to the atmospheric moisture budget. Especially in summer, when the local moisture recycling is to a large degree responsible for precipitation, the decrease in atmospheric moisture is the reason for a reduction in precipitation.

The driver for the changes in the vegetation surface parameters LAI and VGR is the improvement in the phenology simulation for crops. In REMO2009, the crops are "harvested" at a fixed date every year, which is decoupled from the climatic drivers and occurs in late September. The crop phenology in REMO-iMOVE is closely coupled to the atmospheric forcing and thus is able to model the harvest date dynamically. Figure 11 shows the LAI annual cycles of both model versions and the CYCLOPES observation data in 2002 and 2003 for the Cfa and Cfb climate in evaluation region 8 (compare Fig. 3). Evaluation region 8 is located in the area of the described warm deviation. The simulated LAI in REMO-iMOVE depicts very much the characteristics of the observational data, not only in magnitude but also in the timing of maximum and minimum values. REMO2009 is not able to resolve either magnitude, or the timing of maximum or minimum.

GMDD
6, 3085–3135, 2013

5.2 New model features in REMO-iMOVE

In this section we introduce the main advantages of REMO-iMOVE in terms of processes, which the regional model is now able to simulate.

The main advantage is the introduction of plant functional types, which makes it possible to model plant physiological behavior and its direct feedback to the atmosphere. Modeling plant physiological behavior using the described approach in a regional climate model, sets up the basics for climate-ecological experiments in detailed resolution.

The model now takes into account the influence of atmospheric CO_2 concentration to plant stomatal conductance and therefore to surface evaporation. This effect is long known (Betts et al., 1997; Avissar and Pielke, 1991), but so far not modeled in detail, using a high resolution regional climate model.

An advantage in terms of climate variability is the interactive coupling of phenology to climatic drivers. Figure 11 clearly shows this advantage. REMO2009 models a fixed annual LAI and VGR cycle every year, whereas REMO-iMOVE introduces a further source of climate variability by coupling LAI and VGR cycle interactively to its direct atmospherical and soil hydrological drivers.

We consider the net primary productivity (NPP) which is modeled for every plant function type in the grid cell the most important new model output. To model NPP directly in a climate model, driven by all important forcing variables, enables the community to conduct carbon cycle experiments in high resolution, which especially for highly structured terrain or areas with many lakes in the high northern latitudes, is an improvement. In the next section we will evaluate this very important parameter in detail.

5.2.1 Evaluation of modeled net primary productivity

To get insight into the quality of modeled NPP we will compare annual NPP output in detail to literature values for different climate zones in Europe. Usually NPP is measured

GMDD
6, 3085–3135, 2013

in gramm carbon per square meter grid box area per year. NPP is influenced by temperature, soil moisture, solar irradiation, atmospheric CO_2 concentration, and plant development stage expressed by LAI magnitude, hence it is possible to deduce the inter-annual variability from the NPP rates. Representative NPP measurements are rare and also influenced by the inter-annual variability, so the numbers measured are to be handled with care.

We span a range of observations for different plant functional types and compare them to the mean values for each PFT on basis of the evaluation regions. Figure 12 shows annual amounts of NPP per grid-box area of all plant functional types apparent in the climate types of the evaluation regions (compare Fig. 3) for the years 1995 to 2005. Since the growth of some PFTs in REMO-iMOVE is strongly influenced by the water availability, it is useful to compare the NPP values in connection to the amount of soil water.

This connection is evident in nearly all NPP courses in the appendix, located in a semi-arid or arid environment. In the first model year, where the soil hydrology is not in equilibrium with the climate condition, the surplus water evaporates and drains out of the bucket like soil representation. In this time all water sensitive PFTs grow at maximum rates, because the photosynthesis is not limited, neither by water nor by radiation. After this first year, the soil water amounts for all regions is on the same level as in REMO2009 and NPP rates have been adopted to the climate type characteristics.

The growth of certain plants (e.g. grass) is strongly limited by the amount of water present for the plant (Roy et al., 2001). Roy et al. (2001) relate NPP values of tropical grassland to days without water stress per year and found a mostly linear dependence. The NPP rates range between 500–1000 $gC\,m^{-2}$ fresh matter (FM) for about 100 days without water stress, 1000–2000 $gC\,m^{-2}$ FM for about 200 days without water stress and above 3000 $gC\,m^{-2}$ FM for up to 300 days without water stress. Modeled values for the C3 and C4 grass PFTs show values between 0 to 3800 $gC\,m^{-2}\,a^{-1}$ FM for subtropical climate types (Fig. 12 – region 1, 2, 9). Temperate maritime climate types (Fig. 12 – region 3, 4, 5, 6, 7, partly 8) show values between 1300 to 3300 $gC\,m^{-2}\,a^{-1}$ FM.

GMDD
6, 3085–3135, 2013

Temperate continental climate types (Fig. 12 – region partly 8, 10, 11) show a spread between 1300 to 3600 $gC\,m^{-2}\,a^{-1}$ FM. The Boreal regions (Fig. 12 – region 12, 13, 14) show values between 1200 to 2200 $gC\,m^{-2}\,a^{-1}$ FM.

Literature values for the productivity of mediterranean shrub and woodland show an extreme spread. This variability is dependent on vegetation age and the weather conditions in the year, when the measurement was carried out (Roy et al., 2001). A NPP range of 198–1056 gC dry matter $m^{-2}\,a^{-1}$ ($gC\,m^{-2}\,a^{-1}$ DM) is reported for mediterranean shrubland. To convert the measurement to gC fresh matter $m^{-2}\,a^{-1}$ ($gC\,m^{-2}\,a^{-1}$ FM) two factors are applied. The first is the carbon content factor (CF) describes the amount of carbon per plant type and vegetation part and varies between 40–60 %. The second is the dry matter content (DMC) of vegetation especially for shrubs varies between 10–30 % (Roy et al., 2001). Since REMO-iMOVE NPP values are given in gC fresh matter for the whole plant, the dry matter NPP measurements need to be converted by using CF and DMC factors to make them comparable. Applying the maximum and minimum range of measured NPP to the range of CF and DMC values, the comparable NPP rate varies between 366–3771 $gC\,m^{-2}\,a^{-1}$ FM (Table 4).

When comparing simulated shrubland NPP values for evergreen and deciduous shrubs with the values given in Table 4, the simulated values of 1500 to 2500 $gC\,m^{-2}\,a^{-1}$ sit generally in the upper range of observations. In dry years NPP is decreasing to the interval between 200 to 500, which is also shown by observed values. Attention should be paid to the reasons behind the minimum values. In reality vegetation age is important when measuring NPP (Roy et al., 2001). Since the age structure is not modeled in REMO-iMOVE the NPP values generally are overestimated, due to lower productivity in younger shrubland formations (Roy et al., 2001).

The modeled productivity of woodlands for the Mediterranean regions (Fig. 12 – region 1, 2, partly 8, 9) lays between 1000–2000 $gC\,m^{-2}\,a^{-1}$ FM in normal years (the spin up in year 1995 is neglected). In dry years (1999, 2005) the productivity drops drastically below 250 $gC\,m^{-2}\,a^{-1}$ FM and can even reach negative values. Roy et al. (2001) report a range of NPP values for Mediterranean woodlands between 310 to

GMDD
6, 3085–3135, 2013

1750 $gC\,m^{-2}\,a^{-1}$ DM. Roy et al. (2001) also give numbers which are valid for a one year old Quercus Ilex seedling (165 $gC\,m^{-2}\,a^{-1}$ DM), but these can be neglected here, since age is not resolved in the model. Shipley and Vu (2002) report DMC for leave of trees which range approximately between 16 to 42 %. As CF the values of Roy et al. (2001) are assumed. Table 5 shows the spread of mediterranean woodland NPP which is even larger than in shrubs. When comparing to model output, REMO-iMOVE deciduous and coniferous trees generally range in the lower part of observed values.

Literature apportions the productivity of temperate woody species to above and below ground net primary production (ANPP/BNPP). Here we want to check if the modeled values of production fit in the spread of observations when adding ANPP+BNPP.

ANPP measurements for woodlands in temperate climate zone suggest a spread in productivity values, due to different species, stand age and locations. Depending on the nitrogen mineralization, broadleaf and needleleaf species show a distinct spread in above ground productivity. Roy et al. (2001) report measurements form Minnesota and Wisconsin of 200 to 1400 $gC\,m^{-2}\,a^{-1}$ FM for Oak stands, 600 to 900 $gC\,m^{-2}\,a^{-1}$ FM for Mesic Hardwood stands and 400 to 1200 for coniferous tree stands. Depending on mean annual temperature the spread of above ground productivity of a Scot Pine stand in central Poland ranges between about 200 $gC\,m^{-2}\,a^{-1}$ FM at 3 to 5 °C and about 1000 $gC\,m^{-2}\,a^{-1}$ FM at 9 to 11 °C. Another data source for productivity cited in Roy et al. (2001) depicts mean (± one standard deviation) above ground productivity for evergreen coniferous trees in the range of 1000 (± 400.0) $gC\,m^{-2}\,a^{-1}$ FM and deciduous hardwoods in the range of 880 (± 300) $gC\,m^{-2}\,a^{-1}$ FM.

Below ground biomass production essentially consists of the build up of fine roots. Roy et al. (2001) give values between 50 to 400 $gC\,m^{-2}\,a^{-1}$ FM for fine root productivity of different species and locations.

Taking into account all given numbers, the total NPP for temperate zone woodlands range between 250 to 1800 $gC\,m^{-2}\,a^{-1}$ FM. Modeled total NPP values of the humid temperate climate zone (Fig. 12 – regions 3–6) for deciduous and needleleaf trees range between 1000–2400 $gC\,m^{-2}\,a^{-1}$ FM.

GMDD
6, 3085–3135, 2013

Evaluation region 12 to 15 in Fig. 12 define boreal climate types. The modeled NPP values for the woodlands in these regions range between 700–1500 $gC\,m^{-2}\,a^{-1}$ FM. Productivity measurements of Gower et al. (1997) in the BOREAS framework, found aboveground net primary productivity values between approx. 230 and 700 $gC\,m^{-2}\,a^{-1}$ FM with an average value of 420 $gC\,m^{-2}\,a^{-1}$ FM. Below ground root productivity make up approx. 32 % of total productivity in the mean. Here the magnitude is huge, ranging between 3 to 60 % (Roy et al., 2001). Taking the mean value of root productivity combined with the ANPP measurements together spans a range for ANPP+BNPP of 300 to 910 $gC\,m^{-2}\,a^{-1}$ FM for boreal woodlands.

6 Discussion

The one part of REMO2009, which is changed is its surface scheme. These changes in the surface scheme lead to differences in the modeled climate as described in Sects. 5.1.4 and 5.1.5.

The introduction of a lower albedo, due to the increase in forest cover and therefore changes in the snow masking, in the northern part of Europe lead to an increase in 2 m temperature (Sect. 5.1.4). The radiative input in winter is small or even zero in all high northern latitudes. Nevertheless it is enough to influence the surface temperatures. The fact that the cold bias in the described part of the domain in still there in REMO-iMOVE, even if with decreased intensity, leads to the conclusion that other mechanisms apart from the surface variables also play a role in producing the cold deviation in the model. Since this is not the scope of this experiment, we will not further examine the feature.

The intensification of the late summer warm bias in the Balkans region is clearly attributed to the introduction of a crop phenology. The earlier and more intense decrease of the LAI diminishes the latent heat flux and thus the surface cooling. This leads to increased 2 m temperatures. Another feedback, which is visible is a decreased moisture recycling due to less near surface and atmospheric moisture availability. Less atmospheric moisture leads locally to a decrease in precipitation. The moisture recycling

GMDD
6, 3085–3135, 2013

feedback with decreased precipitation is mostly visible in the Hungarian basin and the Balkans in July and August, when the energetic driver – the insolation – reaches its maximum values.

The introduction of the updates in the soil moisture parametrization, did antagonize a more intense increase of surface temperatures due to the possibility of bare soil evaporation. This static method improves the shortcomings of REMO2009, but is not able to capture near realistic soil moisture dynamics like a multi layer soil scheme.

For studies on climate variability, dynamical adjustment of all model parameters to changing climate is vital important. The LAI courses in Fig. 11 and the NPP time series in the appendix clearly show the influence of annual modeled weather characteristics on vegetation growth and productivity.

One of the most important newly introduced parameter in REMO-iMOVE is the NPP. It is crucial for example for studies of the carbon cycle under climate change conditions. In the model, the productivity in dry regions and for certain PFTs is dominantly limited by soil moisture availability. For the C3 grass PFT the modeled NPP values lay in the upper range of observations nearly for all climate types. This would imply water stress free conditions in more than 200 day per year, which is unrealistic for the subtropical and temperate continental climate types. The NPP values in the desert climate of evaluation region 1 (BW/BS) shows nearly zero for all years except the first, where the soil hydrological spin-up took place. Also in evaluation region 2 Csa the NPP rate drops to minimum values in exceptionally dry years (1999, 2000). This is evidence for the functionality of the productivity scheme. The one part which works insufficient in this respect is the soil hydrological scheme. It does not horizontally differentiate the access to water, so plants have direct access to water if it is present in the soil, which is a rather unrealistic assumption. A new hydrological scheme is currently under development, which is able to simulate the horizontal position of water due to the use of multiple layers. Unfortunately this scheme was not ready for use for this study.

The productivity of mediterranean shrubs and woodland is in the range of observations, which is huge. Factors like stand age or nutrition limitation are important for

GMDD
6, 3085–3135, 2013

the growth in these climatic zones and could help to draw a more realistic picture of productivity if incorporated in the model. Nevertheless, the most important factor is the discussed insufficient soil hydrological scheme.

The productivity values of temperate zone woody PFTs range in the upper limits of observations with a tendency of overestimation. The tendency towards too high productivity is likely connected to the fact that nutrient limitation or pests are not modeled in REMO-iMOVE.

The same is true for the productivity in the boreal zone, where REMO-iMOVE overestimates the observed values clearly. The reason here may be either the unsatisfying nutrient limitation or the parameter sets in the photosynthesis scheme controlling the carboxylation and maximum electron transport rate.

7 Conclusions

In this study we coupled the RCM REMO2009 to a 3rd generation surface scheme – namely JSBACH, the surface scheme of the MPI-ESM. REMO2009 and REMO-iMOVE only differ in terms of their surface parameters and parametrizations of surface fluxes and other surface mechanisms.

The use of an interactive vegetation model based on a PFT approach, opens the possibility to treat differences in phenology and plant productivity for a single grid box forced by atmospheric quantities. Due to the inter-annual changes in the atmosphere and its influence on plant phenology, a new source of climate variability is introduced into the RCM now.

NPP is an important parameter for carbon cycle studies. The conduction of carbon cycle studies is now possible in a detailed regional resolution, which is important for example in structured terrain interspersed with lakes – like for example in high northern latitudes.

We analyzed the results of climate simulation for Europe in 0.44° resolution, forced by ERAInterim boundaries for 1995 to 2005, conducted with both model versions. The

GMDD
6, 3085–3135, 2013

simulations show that the new developed model version REMO-iMOVE, is able to simulate the European climate in the same quality as REMO2009 does. The occurring differences reveal the influence of the surface schemes on the modeled climate, which can be distinct in some regions. The main reasons for the different behavior of the two model versions are the different dynamics of vegetation cover and density (VGT and LAI) and the differences in the soil scheme. These parameters influence the surface heat and moisture fluxes in such a way, that the modeled climate shows thorough variation compared to the climate modeled by REMO2009.

We could further show, that the modeled inter-annual variability in the phenology as well as the modeled NPP, is in the range of observations for most European regions examined. Shortcomings occur in regions where the simple soil moisture scheme is not able to capture soil hydrological dynamics influencing plant growth. The direct comparison of the model versions reveals the qualitative gain in modeling LAI dynamics when using REMO-iMOVE.

Apart from the advances introduced, vital importance should be put in the development of a multi layer soil scheme, to correct for the productivity overestimation of solely soil water limited PFTs due to the horizontal ubiquity of soil water but also to improve the underestimation of bare soil evaporation in subtropical and dry central European regions.

Acknowledgements. The work has been carried out at the Max Planck Institute for Meteorology and the Climate Service Center in Hamburg and was funded by the EU FP 7 project ACQWA. The authors posthum thank the patient character of Ralph Podzun, the former chief developer of REMO, for his support in illustrating the technical details of the model REMO. Further we thank C. H. Reick, T. Raddatz and R. Schnur for their support with the JSBACH model.

The service charges for this open access publication
have been covered by the Max Planck Society.

GMDD
6, 3085–3135, 2013

References

Avissar, R. and Pielke, R.: The impact of plant stomatal control on mesoscale atmospheric circulations, Mon. Weather Rev., 117, 213–315, 1991. 3087, 3105

Baret, F., Hagolle, O., Geiger, B., Bicheron, P., Miras, B., Huc, M., Berthelot, B. F. N., Weiss, M., Samain, O., Roujean, J., and Leroy, M.: LAI, FAPAR, and FCover CYCLOPES global products derived from vegetation – Part 1: Principles of the algorithm, Remote Sens. Environ., 110, 305–316, 2007. 3098

Bartholome, E. and Belward, A.: GLC2000: A new approach to global land cover mapping from Earth observation data, Int. J. Remote Sens., 26, 1959–1977, 2005. 3090

Betts, R., Cox, P., Lee, S., and Woodward, F.: Contrasting physiological and structural vegetation feedbacks in climate change simulations, Nature, 387, 796–799, 1997. 3105

Bonan, G.: Ecological Climatology, Cambridge University Press, Cambridge, UK, New York, NY, USA., 2002. 3091

Brovkin, V., Boysen, L., Raddatz, T., Gayler, V., Loew, A., and Claussen, M.: Evaluation of vegetation cover and land-surface albedo in MPI-ESM CMIP5 simulations, J. Adv. Model. Earth Syst., doi:10.1029/2012MS000169, in press, 2012. 3088

Collatz, G., Ribas-Carbo, M., and Berry, J.: A coupled photosynthesis-stomatal conductance model for leaves of C4 plants, J. Plant Physiol., 19, 519–538, 1992. 3093

Davin, E., Stoekli, R., Jaeger, E. B., Levis, S., and Seneviratne, S.: Cosmo-CLM^2: a new version of the COSMO-CLM model coupled to the Community Land Model, Clim. Dynam., 37, 1889–1907, doi:10.1007/s00382-011-1019-z, 2011. 3087

Dickinson, R. E.: Land surface processes and climate-surface albedos and energy balance, Adv. Geophys., 25, 305–353, doi:10.1016/S0065-2687(08)60176-4, 1983. 3093

FAO/IIASA/ISRIC/ISSCAC/JRC: Harmonized World Soil Database (version 1.1), FAO, Rome, Italy and IIASA, Laxenburg, Austria, 2009. 3091

Farquhar, G., von Caemmerer, S., and Berry, J.: A biochemical model of photosynthetic CO_2 assimilation in leaves of C_3 species, Planta, 149, 78–80, 1980. 3093

Garrigues, S., Lacaze, R., Baret, F. J. T. M., Weiss, M., Nickeson, J., Fernandes, R., Plummer, S., Shabanov, N., Myneni, R., Knyazikhin, Y., and Yang, W.: Validation and intercomparison of global leaf area index products derived from remote sensing data, J. Geophys. Res., 113, G02028, doi:10.1029/2007JG000635, 2008. 3098, 3099

GMDD
6, 3085–3135, 2013

Giorgi, F.: Regional climate modeling: status and perspectives, J. Phys., 139, 101–118, doi:10.1051/jp4:2006139008, 2006. 3087
Hagemann, S.: An Improved Land Surface Parameter Dataset for Global and Regional Climate Models, Max-Planck-Institute for Meteorology, Hamburg, Germany, 333 pp., 2002. 3089, 3092
Hagemann, S., Botzet, M., Duemenil, L., and Machenhauer, M.: Derivation of global GCM boundary conditions from 1 km land use satellite data, Max-Planck-Institute for Meteorology, Hamburg, Germany, 289, 1999. 3089
Haylock, M., Hofstra, T., Tank, A., Klok, E., Jones, P., and New, M.: A European daily high-resolution gridded data set of surface temperature and precipitation for 1950–2006, J. Geophys. Res., 113, D20119, doi:10.1029/2008JD10201, 2008. 3098
Holdridge, L.: Life Zone Ecology, Tropical Science Center, San Jose, Costa Rica, 1964. 3090, 3118
Jacob, D.: A note to the simulation of the annual and inter-annual variability of the water budget over the Baltic Sea drainage basin, Meteorol. Atmos. Phys., 77, 61–73, 2001. 3088
Jacob, D. and Podzun, R.: Sensitivity studies with the regional climate model REMO, Meteorol. Atmos. Phys., 63, 119–129, 1997. 3088
Jung, M., Reichstein, M., Margolis, H., Cescatti, A., Richardson, A., Arain, M., Arneth, A., Bernhofer, C., Bonal, D., Chen, J., Gianelle, D., Gobron, N., Kiely, G., Kutsch, W., Lasslop, G., Law, B., Lindroth, A., Merbold, L., Montagnani, L., Moors, E., Papale, D., Sottocornola, M., Vaccari, F., and Williams, C.: Global patterns of land-atmosphere fluxes of carbon dioxide, latent heat, and sensible heat derived from eddy covariance, satellite, and meteorological observations, J. Geophys. Res., 116, G00J07, doi:10.1029/2010JG001566, 2011. 3098
Knorr, W.: Satellite remote sensing and modeling of the global CO_2 exchange of land vegetation: a synthesis study, Examensarbeit Nr. 49, 1998. 3093
Koeppen, W.: Versuch einer Klassifikation der Klimate, vorzugsweise nach ihren Beziehungen zur Pflanzenwelt, Geogr. Z., 6, 593–611, 1900. 3099
Kotlarski, S.: A Subgrid Glacier Parametrisation for Use in Regional Climate Modelling, Max-Planck-Institute for Meteorology, Reports on Earth System Science, Hamburg, 2007. 3089, 3103
Lu, L., Pielke, R., Liston, G., Parton, W., Ojima, D., and Hartman, M.: Implementation of a two-way interactive atmospheric and ecological model and its application to the central United States, J. Clim., 14, 900–919, 2001. 3087

GMDD
6, 3085–3135, 2013

Majewski, D.: The Europa-Modell of the Deutscher Wetterdienst, in: Proceedings of the ECMWF Seminar on Numerical Methods in Atmospheric Models, Reading, UK, 9–13, 147–191, 1991. 3089
Marsland, S., Haak, H., Jungclaus, J., Latif, M., and Roeske, F.: The Max Planck Institute global ocean/sea-ice model with orthogonal curvilinear coordinates, Ocean. Model., 5, 91–127, 2003. 3088
Mitchell, T. and Jones, P.: An improved method of constructing a database of monthly climate observations and associated high-resolution grids, Int. J. Climatol., 25, 693–712, 2005. 3091, 3098
Muller, E. and Decamps, H.: Modeling soil moisture-reflectance, Remote Sens. Environ., 76, 173–180, 2001. 3092
Murray, M., Cannel, M., and Smith, R.: Date of budburst of fifteen tree species in Britain following climate warming, J. Appl. Ecol., 26, 693–700, 1989. 3095
Olson, J.: Global ecosystem framework definitions, USGS EROS Data Center Internal Report, Sioux Falls, SD, 1994. 3089
Peterson, J., Robinson, B., and Beck, R.: Predictability of Change in Soil Reflectance on Wetting, Machine Processing of Remotely Sensed Data Symposium, Laboratory for Applications of Remote Sensing: LARS Technical Reports, Purdue Libraries, 062479, 264–273, 1979. 3092
Pfeiffer, S.: Modeling cold cloud processes with the regional climate model REMO, Max-Planck-Institute for Meteorology, Reports on Earth System Science, Hamburg, 2006. 3089
Pitman, A.: The evolution of, and revolution in, land surface schemes designed for climate models, Int. J. Climatol., 23, 479–510, 2003. 3088
Rechid, D., Raddatz, T., and Jacob, D.: Parameterization of snow-free land surface albedo as a function of vegetation phenology based on MODIS data and applied in climate modelling, Theor. Appl. Climatol., 95, 245–255, 2009. 3089
Reick, C., Raddatz, T., Brovkin, V., and Gayler, V.: The representation of natural and anthropogenic land cover change in MPI-ESM, J. Adv. Model. Earth Syst., 1942–2466, doi:10.1002/jame.20022, 2013. 3088
Roeckner, E., Arpe, K., Bengtsson, L., Christoph, M., Claussen, M., Duemenil, L., Esch, M., Giorgetta, M., Schlese, U., and Schulzweida, U.: The Atmospheric General Circulation Model Echam-4: Model Description and Simulation of the Present Day Climate, Max-Planck-Institute for Meteorology, Report No. 218, 2000. 3089

GMDD
6, 3085–3135, 2013

Roeckner, E., Baeuml, G., Bonaventura, L., Brokopf, R., Esch, M., Giorgetta, M., Hagemann, S., Kirchner, I., Kornblueh, L., Manzini, E., Rhodin, A., Schlese, U., Schulzweida, U., and Tompkins, A.: The atmospheric general circulation model ECHAM 5. PART I: Model description, Max-Planck-Institute for Meteorology, Report No. 349, 2003. 3088

Roy, J., Saugier, B., and Mooney, H.: Terrestrial Global Productivity, Academic Press, New York, 2001. 3106, 3107, 3108, 3109

Rudolf, B. and Schneider, U.: Calculation of Gridded Precipitation Data for the for the Global Land-Surface using in-situ Gauge Observations, in: Proceedings of the 2nd Workshop of the International Precipitation Working Group IPWP, Montery, October, 2004. 3098

Schultz, J.: Die Oekozonen der Erde, UTB, Stuttgart, 2002. 3090

Sellers, P.: Canopy reflectance, photosynthesis and transpiration, Int. J. Remote Sens., 6, 1335–1375, 1985. 3093

Sellers, P., Dickinson, R., Randall, D., Betts, A., Hall, F., Berry, J., Collatz, G., Denning, A., Mooney, H., Nobre, C., Sato, N., Field, C., and Henderson Sellers, A.: Modeling the exchanges of energy, water, and carbon between continents and the atmosphere, Sci. Agric., 275, 502–509, 1997. 3088

Shipley, B. and Vu, T.: Dry matter content as a measure of dry matter concentration in plants and their parts, New Phytol., 153, 359–364, 2002. 3108

Simmons, A., Uppala, S., Dee, D., and Koobayashi, S.: ERA-Interim: New ECMWF reanalysis products from 1989 onwards, ECMWF Newsletter, 110, 26–35, 2006. 3098

Sitch, S., Smith, B., Prentice, I., Arneth, A., Bondeau, A., Cramer, W., Kaplan, J., Levis, S., Lucht, W., Sykes, M., Thonicke, K., and Venevsky, S.: Evaluation of ecosystem dynamics, plant geography and terrestrial carbon cycling in the LPJ dynamic vegetation model, Glob. Change Biol., 9, 161–185, 2003. 3089

Steiner, A., Pal, J., Rauscher, S., Bell, J., Diffenbaugh, N., Boone, A., Sloan, L., and Giorgi, F.: Land surface coupling in regional climate simulations of the West African monsoon, Clim. Dynam., 33, 869–892, 2009. 3087

Stevens, B., Giorgetta, M., Esch, M., Mauritsen, T., Crueger, T., Rast, S., Salzmann, M., Schmidt, H., Bader, J., Block, K., Brokopf, R., Fast, I., Kinne, S., Kornblueh, L., Lohmann, U., Pincus, R., Reichler, T., and Roeckner, E.: The atmospheric component of the MPI-M earth system model: ECHAM6, J. Adv. Model Earth Sci., 1942–2466, doi:10.1002/jame.20015, 2013. 3088

GMDD
6, 3085–3135, 2013

Teichmann, C.: Climate and Air Pollution Modelling in South America with Focus on Megacities, Max-Planck-Institute for Meteorology, Reports on Earth System Science, Hamburg, 2010. 3089

Tsvetsinskaya, E., Schaaf, C., Gao, F., Strahler, A., Dickinson, R., Zeng, X., and Lucht, W.: Relating MODIS-derived surface albedo to soils and rock types over Northern Africa and the Arabian peninsula, Geophys. Res. Lett., 29, 67-1–67-4, 2011. 3091

Warrilow, D., Sangster, A., and Slingo, A.: Modelling of land surface processes and their influence on European climate, Meteorological Office Technical Note DCTN 38, Backnell, UK, 2007. 3089

Weiss, M., Baret, F., Garrigues, S., and Lacaaze, R.: LAI and fAPAR CYCLOPES global products derived from VEGETATION – Part 2: validation and comparison with MODIS collection 4 products, Remote Sens. Environ., 110, 317–331, doi:10.1016/j.rse.2007.03.001, 2007. 3099

Zobler, L.: A world soil file for global climate modelling, Technical Memorandum 87802, NASA, 1986. 3089

GMDD

6, 3085–3135, 2013

Table 1. Ecosystem classification following Holdridge (Holdridge, 1964).

Biotemp [°C]	Precipitation [mm]					
	< 125	125 – < 250	250 – < 500	500 – < 1000	1000 – < 2000	> 2000
< 3	dry tundra (1)	moist tundra (2)	wet tundra (3)	rain tundra (4)	– (5)	– (6)
3 – < 6	desert (7)	dry shrub (8)	moist forest (9)	wet forest (10)	rain forest (11)	– (12)
6 – < 12	desert (13)	desert shrub (14)	steppe (15)	moist forest (16)	wet forest (17)	rain forest (18)
12 – < 24	desert (19)	desert shrub (20)	thorn steppe/ woodland (21)	dry forest (22)	moist forest (23)	wet forest/ rain forest (24)
> 24	desert (25)	desert shrub (26)	thorn steppe/ woodland (27)	very dry forest (28)	dry forest (29)	moist,wet,rain forest (30)

GMDD
6, 3085–3135, 2013

Table 2. Allocation of GLC2000 class mosaic vegetation (grassland/shrubland/forest) (50–70 %)/cropland (20–50 %) to PFTs according to the Holdridge ecosystem classes.

Biotemp [°C]	Precipitation [mm]					
	< 125	125 – < 250	250 – < 500	500 – < 1000	1000 – < 2000	> 2000
< 3	PFT 13: 35 % PFT 12: 30 % PFT 11: 35 %	PFT 13: 35 % PFT 12: 30 % PFT 11: 35 %	PFT 13: 35 % PFT 12: 30 % PFT 11: 35 %	PFT 13: 35 % PFT 12: 30 % PFT 11: 35 %	PFT 13: 35 % PFT 12: 30 % PFT 11: 35 %	PFT 13: 35 % PFT 12: 30 % PFT 11: 35 %
3 – < 6	PFT 13: 40 % PFT 9/10: 60 %	PFT 13: 40 % PFT 9/10: 60 %	PFT 13: 40 % PFT 9/10: 60 %	PFT 13: 40 % PFT 9/10: 45 % PFT 5: 15 %	PFT 13: 40 % PFT 9/10: 40 % PFT 5: 20 %	PFT 13: 40 % PFT 9/10: 40 % PFT 5: 20 %
6 – < 12	PFT 13: 40 % PFT 4: 10 % PFT 5: 10 % PFT 8: 10 % PFT 9/10: 30 %	PFT 13: 40 % PFT 4: 20 % PFT 5: 20 % PFT 8: 10 % PFT 9/10: 10 %	PFT 13: 40 % PFT 4: 20 % PFT 5: 20 % PFT 8: 10 % PFT 9/10: 10 %	PFT 13: 40 % PFT 4: 25 % PFT 5: 20 % PFT 9/10: 15 %	PFT 13: 40 % PFT 4: 25 % PFT 5: 25 % PFT 9/10: 10 %	PFT 13: 40 % PFT 4: 30 % PFT 5: 30 %
12 – < 24	PFT 13: 40 % PFT 9/10: 60 %	PFT 13: 40 % PFT 7: 35 % PFT 9/10: 25 %	PFT 13: 40 % PFT 4: 20 % PFT 5: 15 % PFT 7: 15 % PFT 9/10: 10 %	PFT 13: 40 % PFT 4: 25 % PFT 5: 10 % PFT 7: 15 % PFT 9/10: 10 %	PFT 13: 40 % PFT 4: 20 % PFT 5: 20 % PFT 7: 20 %	PFT 13: 60 % PFT 4: 20 % PFT 5: 20 % PFT 7: 20 %
> 24	PFT 13: 40 % PFT 7: 30 % PFT 9/10: 30 %	PFT 13: 40 % PFT 7: 30 % PFT 9/10: 30 %	PFT 13: 40 % PFT 2: 10 % PFT 7: 50 %	PFT 13: 40 % PFT 2: 40 % PFT 7: 20 %	PFT 13: 40 % PFT 1: 40 % PFT 7: 20 %	PFT 13: 40 % PFT 1: 50 % PFT 8: 10 %

GMDD
6, 3085–3135, 2013

Table 3. Koeppen–Geiger climate types used for model evaluation.

B	Arid climates
BSh	Hot steppe climate
BSk	Cold steppe climate
BWh	Hot desert climate
BWk	Cold desert climate
C	Warm temperate climates
Csa	Warm temperate climate with dry hot summer
Csb	Warm temperate climate with dry warm summer
Cfa	Warm temperate climate fully humid with hot summer
Cfb	Warm temperate climate fully humid with warm summer
Cfc	Warm temperate climate fully humid with cold summer
D	Snow climates
Dsb	Snow climate summer dry, warm summer
Dsc	Snow climate summer dry, cold summer
Dfa	Snow climate fully humid, hot summer
Dfb	Snow climate fully humid, warm summer
Dfc	Snow climate fully humid, cold summer
E	Polar climates
ET	Tundra climate
EF	Frost climate

GMDD
6, 3085–3135, 2013

Table 4. NPP range of shrubland, when converting from $gC\,m^{-2}\,a^{-1}$ DM to $gC\,m^{-2}\,a^{-1}$ FM.

g dry matter	g carbon fresh matter	
	minimum DMC/CF 10 % / 40 %	maximum DMC/CF 30 % / 60 %
198	366	707
1056	1955	3771

GMDD
6, 3085–3135, 2013

Table 5. NPP range of Mediterranean woodlands, when converting from $gC\,m^{-2}\,a^{-1}$ DM to $gC\,m^{-2}\,a^{-1}$ FM.

g dry matter	$gC\,m^{-2}\,a^{-1}$ FM	
	minimum DMC/CF 16 % / 40 %	maximum DMC/CF 42 % / 60 %
310	615	1614
1750	3472	9114

GMDD
6, 3085–3135, 2013

Table 6. Dependence of the litter albedo scaling factor on the plant functional type (PFT).

PFTs	$\varkappa$	PFTs	$\varkappa$	PFTs	$\varkappa$
1–3	3	9–11	1	13	3
4–8	2	12	4	14–16	0

GMDD
6, 3085–3135, 2013

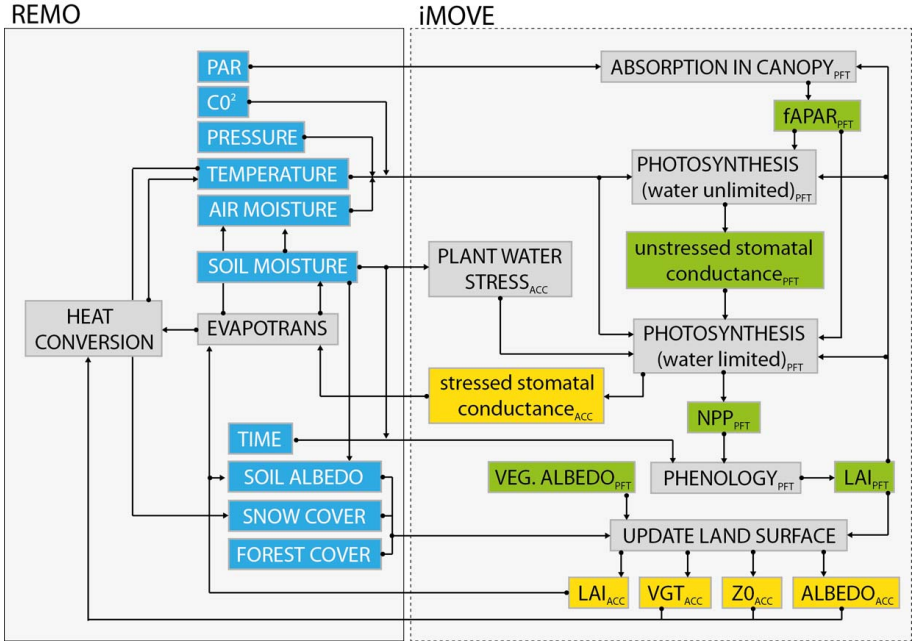

Fig. 1. Coupling concept of REMO-iMOVE.

GMDD
6, 3085–3135, 2013

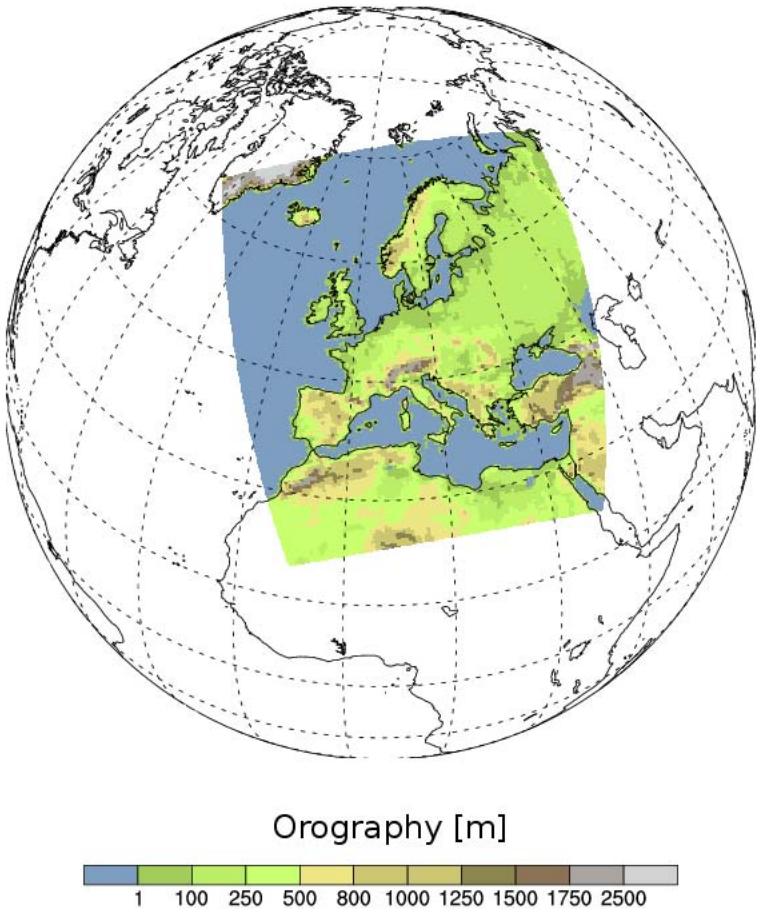

Fig. 2. Domain of the reference climate model runs with REMO2009 and REMO-iMOVE.

GMDD
6, 3085–3135, 2013

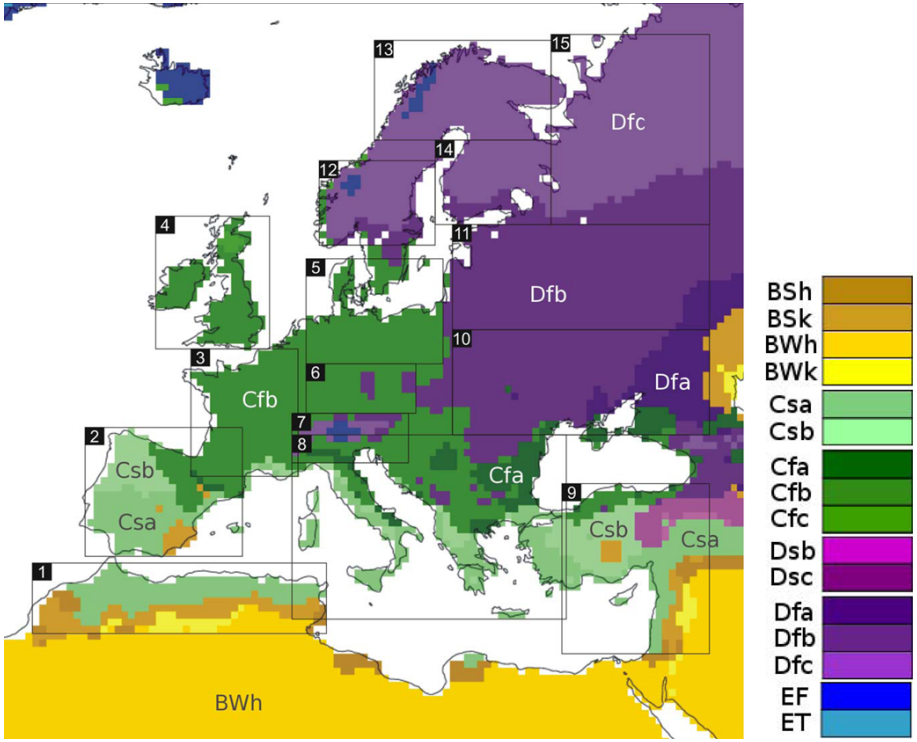

Fig. 3. Climate types based on the Koeppen–Geiger climate classification and evaluation regions for the model domain.

GMDD
6, 3085–3135, 2013

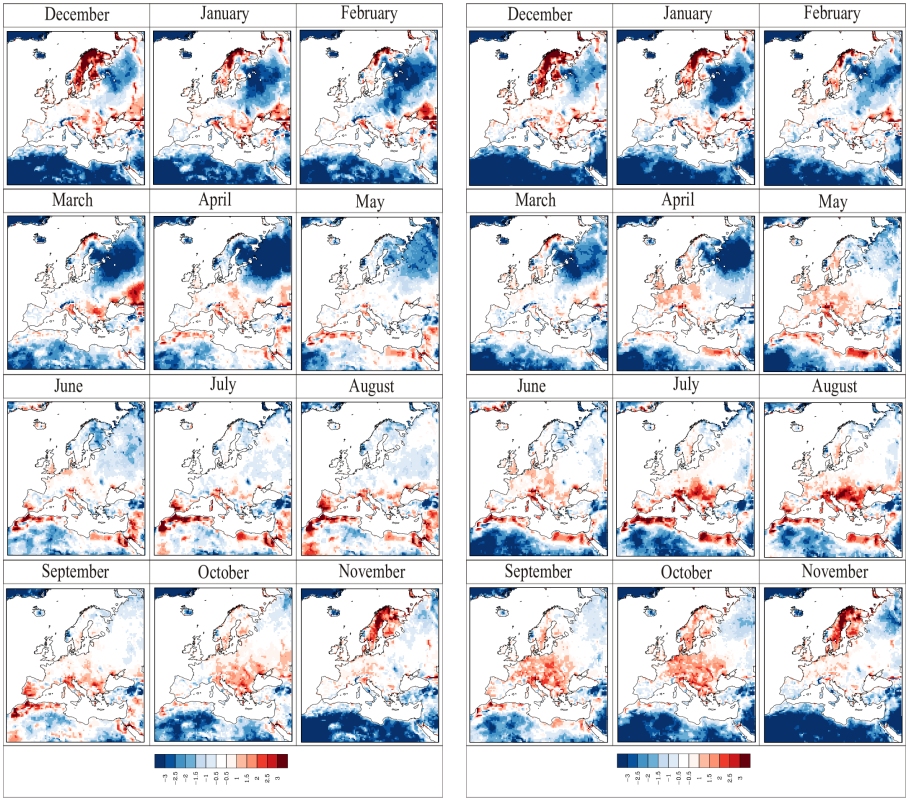

Fig. 4. Differences of 2m-T of REMO2009 vs. CRU and REMO-iMOVE vs. CRU in the period 1996 to 2005.

GMDD
6, 3085–3135, 2013

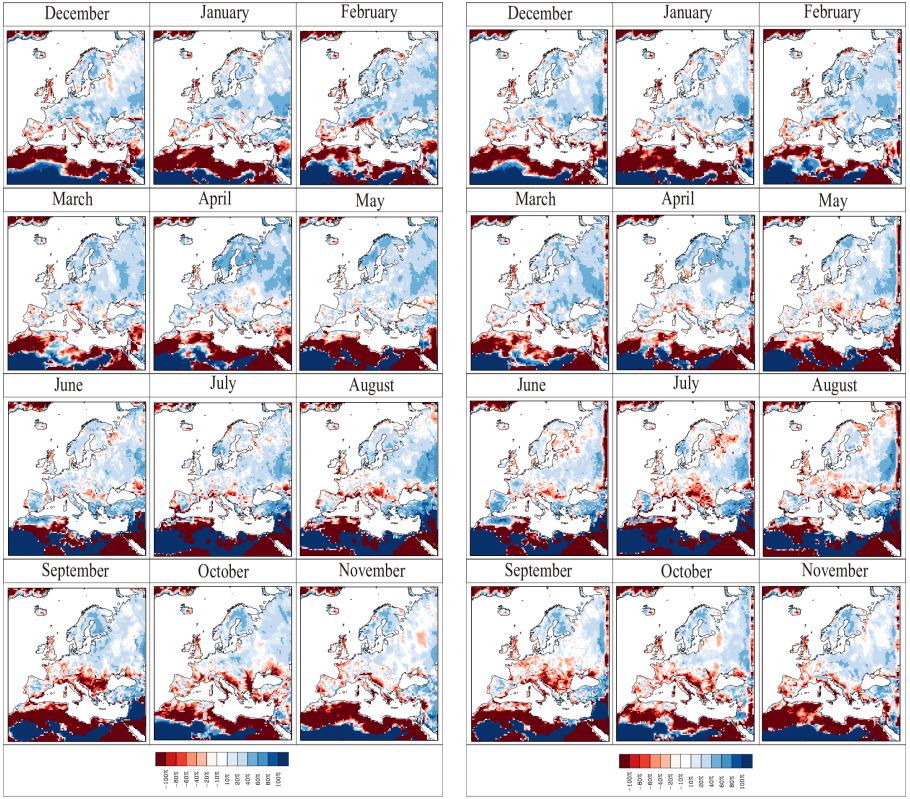

Fig. 5. Differences of total precipitation of REMO2009 vs. CRU and REMO-iMOVE vs. CRU in the period 1996 to 2005.

GMDD
6, 3085–3135, 2013

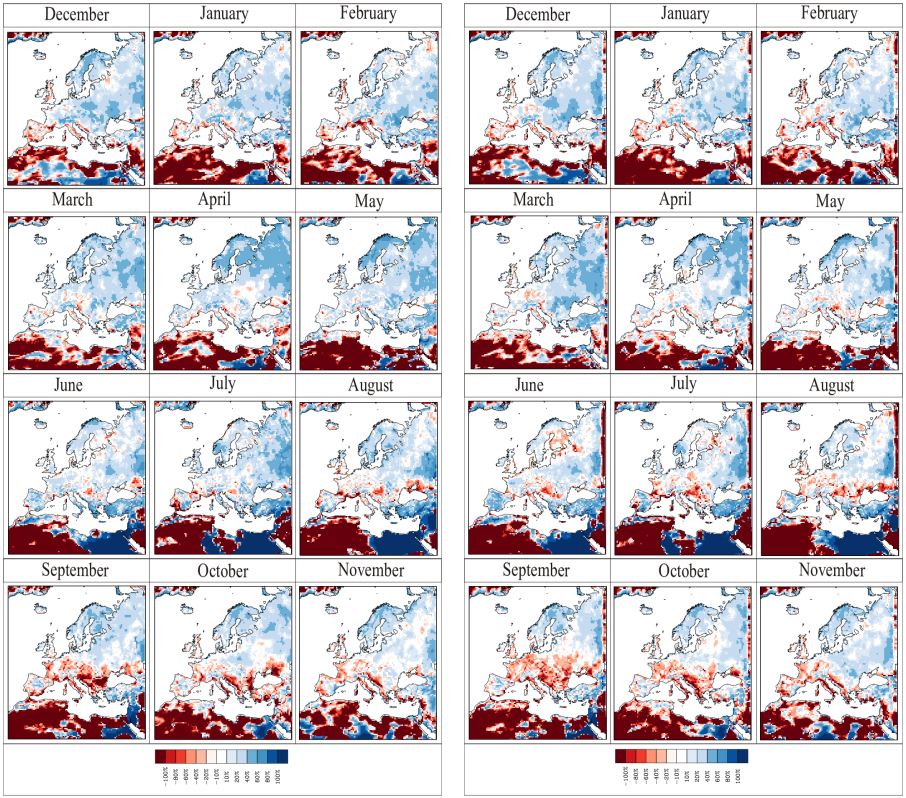

6 a) REMO2009 - CRU

6 b) REMO-iMOVE - CRU

Fig. 6. Differences of total precipitation of REMO2009 vs. GPCC and REMO-iMOVE vs. GPCC in the period 1996 to 2005.

GMDD
6, 3085–3135, 2013

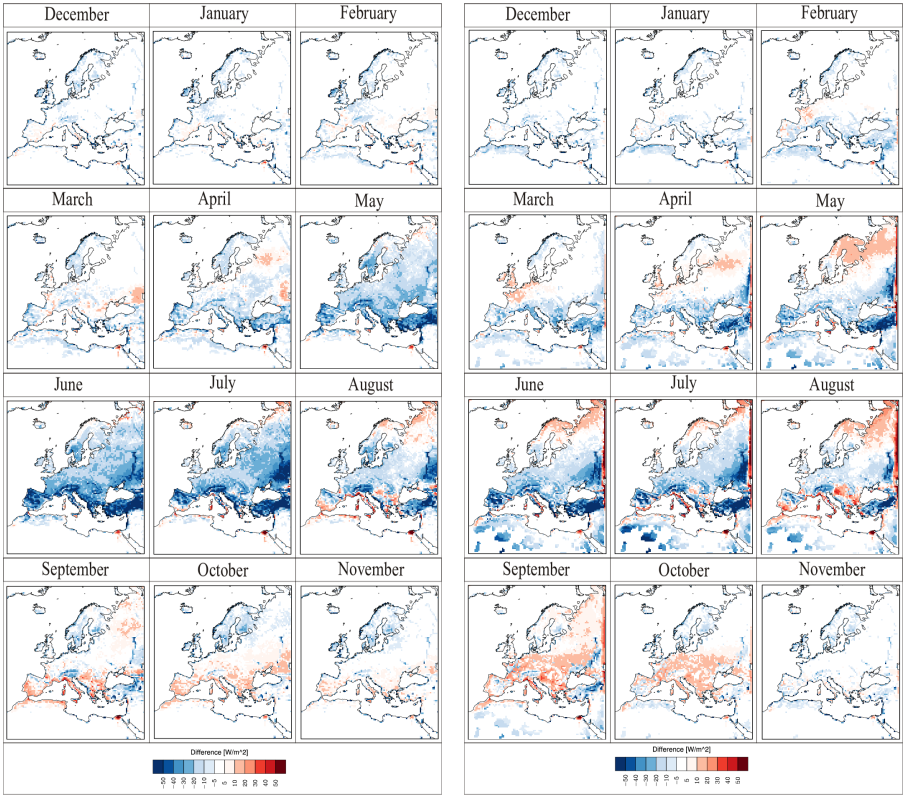

Fig. 7. Differences of surface latent heat flux of REMO2009 vs. FLUXNET and REMO-iMOVE vs. FLUXNET in the period 1995 to 2001.

GMDD
6, 3085–3135, 2013

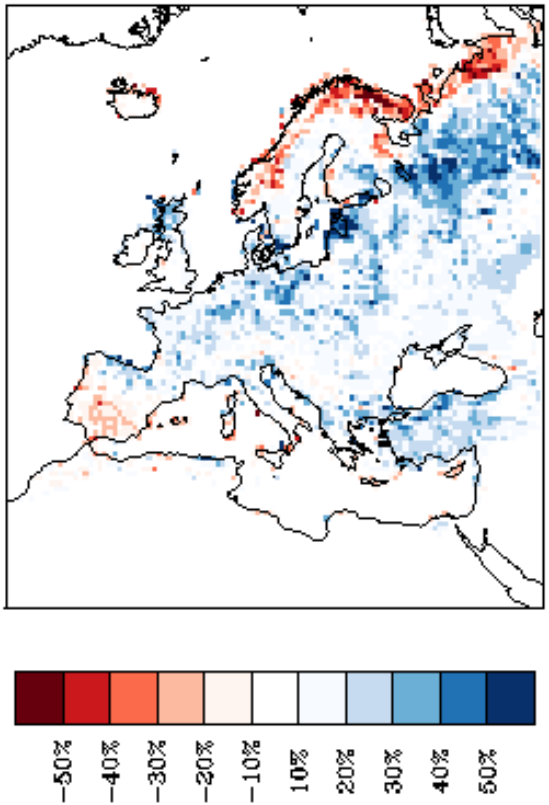

Fig. 8. Differences in forest cover between REMO-iMOVE and REMO2009.

GMDD
6, 3085–3135, 2013

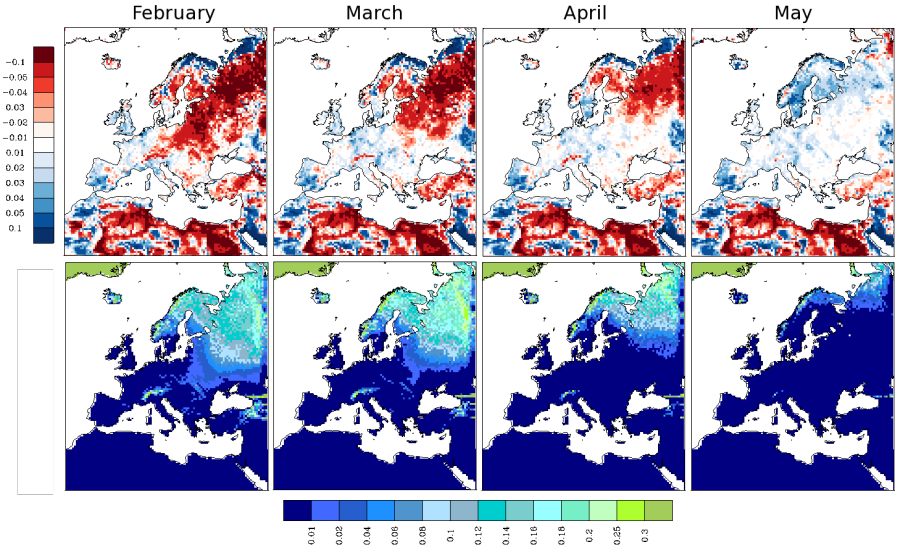

Fig. 9. Differences in albedo between REMO-iMOVE and REMO2009 in reflectance percent (upper row), snow depth in REMO-iMOVE in meter (lower row).

GMDD
6, 3085–3135, 2013

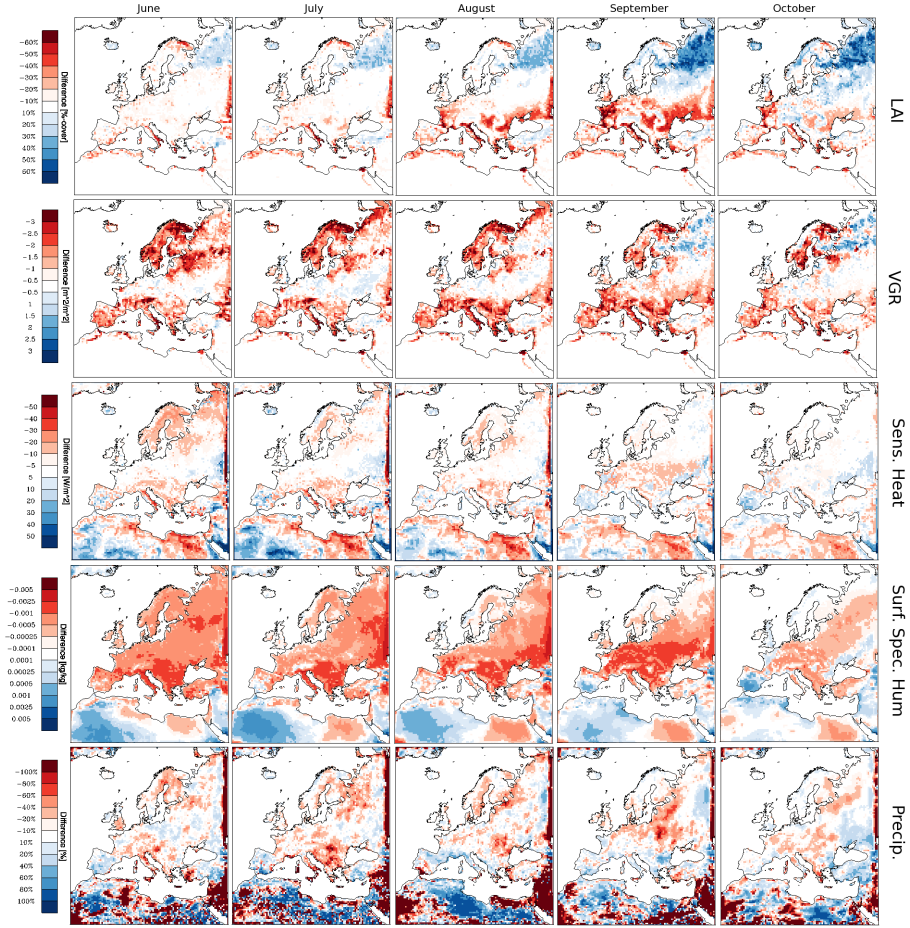

Fig. 10. Differences in model parameters (LAI, vegetation ration (VGR), sensible heat flux, surface specific humidity, precipitation) from June to October.

GMDD
6, 3085–3135, 2013
REMO-iMOVE
C. Wilhelm et al.

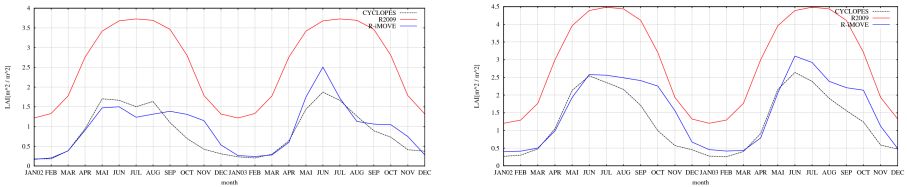

Cfa Cfb

Fig. 11. Annual course of LAI in 2002 and 2003 of REMO-iMOVE, REMO2009 and CYCLOPES in the Cfa and Cfb climate of evaluation region 8 (compare Fig. 3).

GMDD
6, 3085–3135, 2013

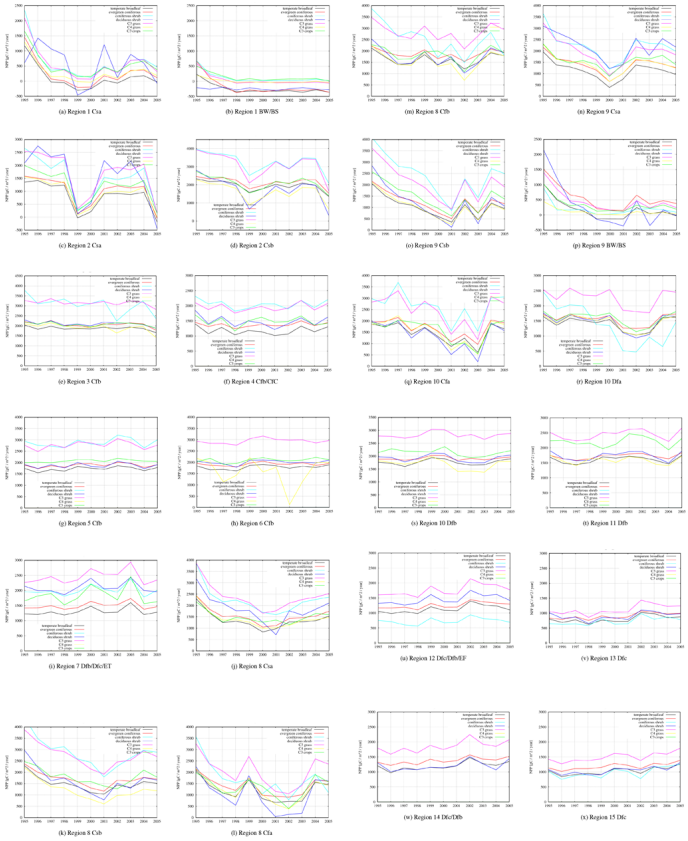

Fig. 12. Net primary productivity [g C m^{-2} yr^{-1}] variations in the evaluation regions in the period 1995 to 2005.

GMDD
6, 3085–3135, 2013